and together with the change in magnetization are tabulated in Table I. The error in these numbers is estimated to be less than 10% at the lowest temperatures, increasing to about 30% above 1.0°K. The values of ΔM and l at 1.256° K are probably too large. It was difficult in this case to judge how much area to include in the ΔM calculation due to the broadness of the peak and the small separation between the two transitions. If ΔM and l are extrapolated to zero at 1.30°K, then the quoted values of these quantities at 1.256°K fall well above the smooth curve.

It might be well to point out, in conclusion, that according to Anderson and Callen[10] the temperature dependence of the SF-to-P transition boundary should determine how spin-wave renormalization should be carried out. That is, if spin-wave energies are renormalized by the energy then the temperature dependence should be $T^{5/2}$; however a $T^{3/2}$ dependence is expected if the energy is renormalized by the magnetization. Our results show that the actual dependence is $T^{1.82}$ which would indicate that the $T^{3/2}$ term is dominant.

The author wishes to express his gratitude to the Oak Ridge Associated Universities and Oak Ridge National Laboratory (ORNL), whose support, through a Research Participation Grant, made this work possible; to Derek Walton of ORNL for the use of his research equipment and for many helpful discussions; to the ORNL x-ray diffraction group for the crystal orientation data; and to John H. Henkel for many helpful discussions.

PHYSICAL REVIEW VOLUME 162, NUMBER 2 10 OCTOBER 1967

Spin-Echo and Free-Induction-Decay Measurements in Pure Fe and Fe-Rich Ferromagnetic Alloys: Domain-Wall Dynamics

MARY BETH STEARNS
Scientific Laboratory, Ford Motor Company, Dearborn, Michigan

(Received 31 October 1966; revised manuscript received 8 May 1967)

Measurements were made of the free-induction-decay (FID) and spin-echo amplitudes of Fe^{57} in pure Fe and some of its alloys. Complex spectra are observed consisting of many oscillations often covering a range of many Mc/sec. The amplitudes are very dependent on the pulse length τ, the applied rf field B_1, and the exciting frequency ω. Excellent agreement is found between the experimental and calculated amplitudes when a model for domain-wall motion is used which takes into consideration the following features: 1. There is an averaging over the orientation of $\mathbf{B}_1$ with respect to the local magnetization. 2. There is a variation of the enhancement factor across the domain wall due to the spin arrangement in the wall. 3. The domain wall is considered to be composed of area segments which are immobile along their perimeters and whose motion resembles that of a vibrating drumhead. 4. These domain-wall segments have a distribution in areas. The restricted motion of the domain walls imposed by the last two features is essential in order to obtain agreement with the experimental results. This is in contrast to the usual model, which represents the domain-wall motion as given by rigid simple-harmonic-like oscillations; such a model shows great discrepancy with the experimental results presented here. In some of the spectra, asymmetries are observed in the variation of the amplitudes as a function of frequency. No satisfactory explanation for these asymmetries is known although some possible sources are suggested. Such asymmetries make it appear very doubtful that the Fe-alloy spectra obtained with this technique can be reliably unfolded to give the variation of the internal field for second- or higher-neighbor impurity atoms. FID amplitude measurements were also made on Fe in an externally applied dc field. No variation in the value of the maximum enhancement factor was observed for dc fields varying from 0 to about 5 kG.

I. INTRODUCTION

SEVERAL investigators[1–3] have been using spin-echo techniques to try to measure the variation of the internal field at different occupational configurations in ferromagnetic alloys. The hope is then to correlate the measured internal fields with the various neighbor shells of solute atoms and thus obtain the spin-density variation as a function of distance from the magnetic ion. When measurements were made on the same Fe alloys with both NMR (Nuclear Magnetic Resonance) and Mössbauer techniques,[3,4] it was found that the two methods did not give the same shifts for second- and third-nearest neighbors and, moreover, that the shape of the spectra obtained with NMR did not vary in a manner consistent with the calculated abundance of the various occupa-

[1] (a) R. F. Jackson, R. G. Scurlock, D. B. Utton, and T. H. Wilmsburst, Phys. Letters **11**, 197 (1964); **12**, 168 (1964). (b) S. Kobayashi, K. Asayama, and J. Itoh, J. Phys. Soc. Japan **21**, 65 (1966). (c) J. I. Budnick, S. Skalski, T. J. Burch, and J. H. Wernick, J. Appl. Phys. **38**, 1137 (1967).

[2] R. L. Streever and G. A. Uriano, Phys. Rev. **139**, A135 (1965); **149**, 295 (1966).

[3] M. Rubinstein, G. H. Stauss, and M. B. Stearns, J. Appl. Phys. **37**, 1334 (1966).

[4] M. B. Stearns, Phys. Rev. **146**, 439 (1966).

tional configurations as the solute-atom concentration was varied. Since the NMR behavior of ferromagnetic materials is itself quite complex, it was believed that the spectra of pure Fe should be studied more carefully to learn more about what is occurring in these pulsed experiments. In ferromagnetic NMR experiments[5–8] the main signal appears to arise from the nuclei in the domain walls, the nuclei in the domains being more or less completely shielded from the applied rf field when walls are present. Moreover, the rf field is enhanced by a factor of about 10^3 in Fe. Part of this results from the circumstance that the internal magnetic field as seen by the Fe^{57} nuclei is about 200 times the static-anisotropy field acting on the electrons and part is due to further enhancement from wall motion.

Extensive measurements were made of the dependence of the free-induction-decay amplitude (FID) and the spin-echo amplitude on the frequency ω, field strength B_1, and pulse length τ, at various temperatures and external fields. The spectra obtained are indeed quite complex and depend strongly on the product $B_1\tau$ and ω. The FID measurements are easier to interpret and from them much information can be obtained about the structure and motion of the domain walls. This is discussed in Sec. III B. The spin-echo results confirm the FID findings and they are discussed in Sec. IV. The experimental results were not consistent with the usual model of rigidly oscillating domain walls even though proper account was taken of the B_1 orientation and the enhancement-factor distribution perpendicular to the plane of domain-wall due to the spatial arrangement of the spins in the wall. They were consistent with a model that had the added restriction that each domain-wall was considered immobile along its perimeter. A wall oscillation thus resembles that of a vibrating drumhead. Furthermore, the average enhancement factor of each wall is proportional to its area. Thus, a distribution in domain wall areas must be incorporated into the model. This model is discussed in Sec. III B3. Except for some observed asymmetries in some of the spectra, the drumhead model gives excellent agreement with the observed data.

Many of the features observed in the pure Fe spectra are also evident in the spectra of Fe alloys. This makes the alloy spectra very difficult, if not impossible, to interpret in terms of the internal field due to impurity atoms in second or higher-neighbor shells. The alloys are discussed in Sec. V.

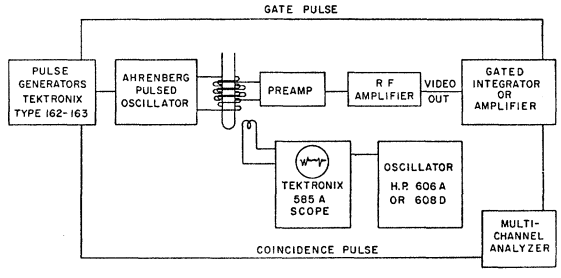

FIG. 1. Schematic diagram of experimental apparatus.

II. EXPERIMENTAL PROCEDURE

The experimental apparatus was similar to that used by other experimenters,[2] with the exception that the data were recorded on a multichannel analyzer operating in the coincidence mode. Figure 1 shows a schematic diagram of the experimental arrangement. An Ahrenberg Ultrasonic Laboratory Model PG 650-C, pulsed oscillator was externally pulsed by a wave train generated by Type 162 and 163 Tektronix pulse generators. There is thus no phase sensitivity in this apparatus. The pulse length of the rf pulses was varied between $\frac{1}{2}$ and 15 μsec for various measurements. The rf magnetic field with Fe in the transmitter coil could be varied from about 0.2 to 8 G. The measurements were made at liquid He, liquid N_2, and room temperatures in external fields varying from 0 to 8 kG. Powdered samples of various shapes and sizes were used. The preamplifier and receiver were extensively modified versions of those described by Clark.[9] The quenching system used was simply two back to back FD100 diodes at the input of the preamp. These worked very well and gave a recovery time of about 3–5 μsec. The transmitter and receiver coils were coaxial. The receiver coil was connected to the preamplifier through a half-wavelength coaxial cable terminated in its characteristic impedance. The video output of the receiver was fed into a Tektronix Type O operational-amplifier unit which was used as an amplifier or inverter when measuring the free-induction decay and sometimes the echo or as a gated integrator when measuring the echo. The echo was usually integrated to avoid difficulties arising from the shape dependence of the echo due to turning-angle effects.[10] The output of the operational amplifier was fed into the multichannel analyzer which was made operational by a 5 μsec coincidence pulse. This pulse was adjusted to occur at whichever time we desired to measure the FID or echo amplitude. The frequencies were measured by beating the rf signals against the output of a 606 A or 608 D Hewlett Packard oscillator

[5] A. M. Portis and A. C. Gossard, J. Appl. Phys. **31**, 205S (1960)
[6] J. I. Budnick, L. J. Brunner, R. J. Blume, and E. L. Boyd, J. Appl. Phys. **32**, 120S (1961).
[7] M. Weger, E. L. Hahn, and A. M. Portis, J. Appl. Phys. **32**, 124S (1961).
[8] A. M. Portis and R. H. Lindquist, in *Magnetism*, edited by G. T. Rado and H. Suhl (Academic Press Inc., New York, 1965), Vol. 2A, p. 357.
[9] W. G. Clark, Rev. Sci. Instr. **35**, 316 (1964).
[10] W. B. Mims, Phys. Rev. **141**, 499 (1966). The effects reported here are not the same as those discussed by Mims. He was concerned with the shapes of the spin-echo signals in a system where the linewidths were wide compared to the rf field intensity H_1. We are mainly concerned with the spin-echo amplitude for lines which are narrow compared to the rf field intensity. Here, because of the enhancement factor, the rf field intensity at the nucleus is 10kG or less, whereas the Fe linewidth is about 0.4kG.

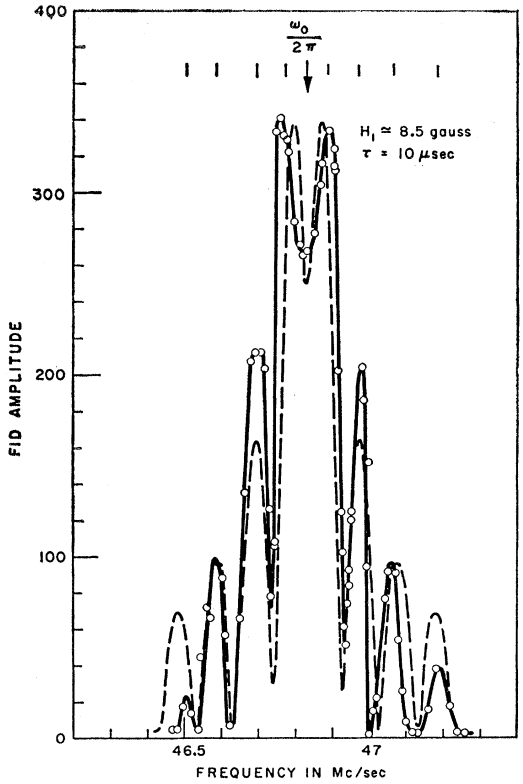

FIG. 2. Variation of the FID amplitude with exciting rf frequency for protons in lucite. The turning angle at resonance, $\gamma H_1 \tau = 2.3$ rad. The dashed curve is that calculated from Eq. (1).

and reading the frequency with an electronic counter; they could be easily and reproducibly determined to 10 kc/sec.

It should be emphasized that in an experiment of this type almost all the variables having to do with the experimental apparatus are interdependent. For example, the frequency of the oscillator depends on the rf power level and the value of an external magnetic field, if present. Thus, extreme caution must be taken throughout the experiment to check all variables and make readjustments when changing any variable.

III. FID RESULTS

In general, two types of measurements were made on both the FID and spin-echo amplitudes. In the first type (I), the amplitudes were measured as a function of transmitting frequency ω, with the rf power level H_1, and the pulse length τ, held essentially constant. In the second type (II), ω and τ were held constant and the amplitudes were measured as a function of H_1. Here, ω was usually kept at the resonant frequency ω_0.

We shall first discuss the FID amplitudes since they are simpler to compare with theory and also larger in magnitude and therefore easier to measure. In these experiments, we apply the rf pulse for a time τ and observe the height of the video pulse at some time after the end of the rf pulse. We ascertained that the spectra obtained were essentially independent of the time at which the FID was sampled by measuring the spectra at various times after the end of the rf pulse. The rf pulses were nearly square except at the highest powers, where they were somewhat rounded at the front of the pulse. Their quality was examined by frequency analyzing them with a Tektronix Type 1L20 Spectrum Analyzer. These measurements yielded exemplary patterns of the Fourier transform of a nearly square pulse.

A. Protons

In order to separate clearly which effects in an experiment of this type are due to ferromagnetic behavior and which are more normal effects and to check that the experimental apparatus was behaving as expected, we made measurements on protons in a lucite rod at room temperature. A dc magnetic field was applied at right angles to the linearly polarized rf field produced in the transmitting coil and we measured the height of the FID. The dc field was adjusted to give a resonance at about the same frequency as the Fe resonance. We measured the height of the FID about 15 μsec after the end of the rf pulse. The solid line in Fig. 2 shows the measured variation in the height of the FID with transmitting frequency ω. The experimental points have been corrected for the variation in gain of the preamp and receiver. Although the nuclei are forced to resonate at the transmitting frequency when the rf pulse is on, as soon as it goes off, they resonate at their own frequency $\omega_0 = \gamma_p H_{dc}$. Thus, the gain correction needed is that obtained by measuring the gain at frequency ω_0 with the transmission frequency set at ω. Since we have tightly coupled transmitting and receiving coils, this variation is quite different from the gain of a signal of frequency ω with the same transmission frequency.

The dashed curve is the expected FID spectrum. It is calculated in the following manner. We use the usual notation as given, for example, in Refs. 11 and 17. The rf field is linearily polarized, i.e., $H_{rf} = 2H_1 \sin\omega\tau$. We are interested in only one rotating component, so H_1 is

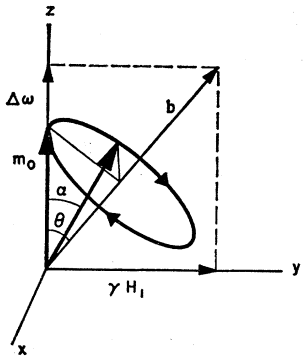

FIG. 3. Diagram of the precession cone in the rotating reference frame.

[11] A. Abragam, *The Principles of Nuclear Magnetism* (Clarendon Press, Oxford, 1961) p. 20.

TABLE I. Purity, size, and enhancement factors of the Fe samples.

Sample	Type	% Fe	Size and shape	ϵ_0
1	Johnson-Matthey	99.999	1–10μ needlelike	~6000 (4.2°K) ~8500 (78°K) ~19000 (298°K)
2	GAF[a] *L*	99.5	6–9μ spheres	~2800 (4.2°K)
3	GAF[a] GS-6	99.0	3–5μ spheres	~2000 (4.2°K)

[a] General Aniline and Film Corporation; other constituents are C, N, and O.

the amplitude of the applied rf. As usual, we go into the reference frame rotating at a frequency ω. Then the nuclei experience a fictitious field in the direction of the dc field (z) of magnitude $\Delta\omega/\gamma$, where $\Delta\omega=\omega-\omega_0$. In the rotating frame let the rf field direction be taken as the y axis. Then, when the rf field is on, the nuclei precess about the resultant vector $\mathbf{b}$ which makes an angle θ with respect to the z axis, as shown in Fig. 3. The angle through which the nuclear moment $\mathbf{m}_0$ turns is given by $b\tau$. This corresponds to the nuclear-moment vector turning through a space angle α. After the rf pulse is turned off, the nuclear moment freely precesses about the direction of the dc magnetic field at frequency ω_0. The receiving coil is collinear with the transmitting coil and is therefore sensitive to the component of the nuclear moment in the x-y plane. This component is given by

$$\mathcal{A}(\omega)=m_0\sin\alpha=m_0\sin\theta[\sin^2 b\tau+\cos^2\theta(1-\cos b\tau)^2]^{1/2}, \quad (1)$$

where

$$\tan\theta=\gamma H_1/\Delta\omega, \quad (2)$$

and the turning angle is

$$b\tau=[(\Delta\omega)^2+(\gamma H_1)^2]^{1/2}\tau. \quad (3)$$

For the spectrum shown in Fig. 2, H_1 was measured to be 8.5 G and τ was 10 μsec, corresponding to a turning angle at resonance of $\gamma H_1\tau=2.3$ rad. The dashed curve in Fig. 2 is calculated from Eq. (1) using the above values. It is seen that the agreement with the experimental points is very good; the more rapid falloff of the experimental points than the calculated curve in the wings of the spectrum is due to the nonlinearity of the video-diode detector for small signals. The deviations between the two curves near resonance is probably due to the fact that the calculated curve is for a square rf pulse, whereas the actual rf pulse is slightly rounded off since here we had to take the data at maximum rf power in order to see the oscillations. A few features of the spectrum should be emphasized. The hole dug at resonance is due to having a turning angle at resonance of greater than 90°. The depth of the hole should oscillate as the turning angle varies through multiples of π. Unfortunately, this second type measurement could not be made with the protons since the hole depth could not be measured accurately at the large τ's (and therefore narrow frequency range for the hole) needed for these measurements. The oscillations off resonance also reflect the periodic variation of the turning angle, but here they occur with a turning angle period of 2π. From Fig. 3 we can see that when we are off resonance, we get a maximum x-y component of m_0 every time the turning angle is an odd multiple of π and no x-y component whenever the turning angle is an even multiple of π. The larger the value of the turning angle at resonance, the more oscillations we can see. For regions of the spectra which have small θ, i.e., when $\gamma H_1/\Delta\omega\ll 1$, Eq. (1) gives a shape corresponding to the Fourier transform of the transmitting pulse. The measured proton spectra are thus understood and are well described by Eq. (1).

B. Iron

1. Experimental Spectra; Type-I Measurements

Let us now consider the FID spectra of Fe. Measurements were made on various Fe samples whose size, shape, and purity are listed in Table I. The impurities were mainly C, N, and O and are assumed to be mainly in interstitial positions. The transverse relaxation time of the samples at He temperatures was measured to be about 8 msec from the decrease of the echo intensity. The spin-lattice relaxation time T_1 is about 0.6 sec.[7] At He temperatures, we used a repetition rate of 800 msec; the FID amplitude did not increase at longer repetition rates. The FID decay time was 15–20 μsec for the Fe samples listed in Table I. Measurements of the FID were also made at liquid N_2 and room temperature. The FID height was usually measured about 10 μsec after the end of the rf pulse although other times were also used and the spectra were independent of this sampling time. The left-hand side of Fig. 4 shows some typical spectra of the FID amplitude as a function of the rf transmitting frequency for sample 1. Many other spectra were taken under a great variety of conditions and their features agree with the description given below. When necessary, these curves have been corrected for the gain change measured with the received signal at ω_0 while the exciting frequency was ω; there should be no other frequency dependencies. Most of the Fe data were taken after the receiver system was improved, so that there was little or no variation in gain

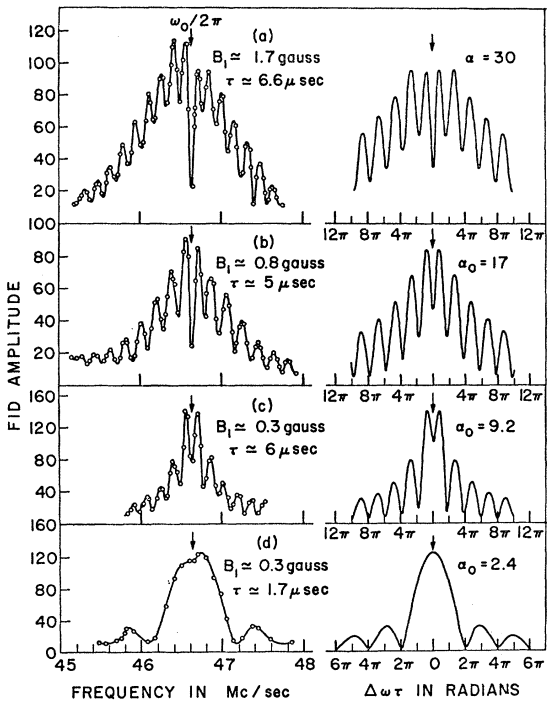

FIG. 4. Typical spectra of FID amplitude as a function of trasmitting frequency for fixed B_1 and τ for sample 1. The left-hand side shows some measured spectra. The right-hand side shows spectra calculated with the drumhead model of domain-wall motion as given by Eq. (18′) with $A\ p(A)=\text{const}$.

with change in the transmission frequency. The video-detector system was also improved after the proton data were taken. Thus, for the Fe data, it was essentially linear over the range used. We checked that the frequency of the FID signal was always ω_0, i.e., independent of the exciting frequency in two ways: (1) by beating the FID signal against the pulsed output of a 608D Hewlett Packard oscillator and, (2) by frequency analyzing the FID on the 1L20-spectrum analyzer. At each temperature, the frequency remained the same to within 20 kc/sec over the entire range of transmitting frequencies, B_1's or τ's which were available. The resonant frequency values obtained at the various temperatures are listed in Table II and agree well with those of Ref. 6. The ratio of the signal strength at 4.2°K to that at 78°K was about as expected for a $1/T$ dependence of the nuclear susceptibility. The spectra shown in Fig. 4 were taken at 4.2°K.

2. *FID Amplitude at Resonance; Type-II Measurements*

These measurements were made by varying B_1 with the transmitting frequency held at ω_0 and τ fixed.[12] Since we want to measure the amplitude of the minimum of the hole accurately, it is necessary to keep τ small. We used $\tau \leq 3$ μsec. Figure 5 shows experimental data obtained with τ values of 1.2 and 3 μsec for sample 1. Under no conditions did we ever observe the hole depth to oscillate; it always rose to a maximum and then gradually decreased as shown in Fig. 5. All of the measurements could be fitted to a universal curve of FID amplitude versus B_1. However, the scale factor of the abscissa B_1 depended on the purity and temperature of the samples. As we shall see, this means the maximum enhancement factor varied with sample and temperature. We found that the higher the impurity content the lower was the maximum-enhancement factor. For sample 1, we observed that the higher the temperature, the larger was the maximum enhancement factor. Both of these behaviors are easily understood in terms of the model proposed below. The measured maximum enhancement factors are listed in Table I. We discuss the comparison of the observed data with the calculated curves shown in Fig. 5 in the next section.

3. *Calculated Spectra*

We calculate the expected FID spectrum by the proper modifications of Eq. (1). This involves: averaging over the angle between the rf field and the directions of magnetization in the Fe, and taking into account the variation of the enhancement factors in the domain walls.

a. Averaging over B_1 orientation (constant ϵ). At zero-applied external field, the local fields in the Fe powder are assumed to be isotropically distributed about the rf fields. Let us consider an Fe atom whose static anisotropy field H_A is pointing in the z direction which makes an angle η with respect to the direction of the rf field B_1. All the B_1 values quoted were measured by the voltage induced in a single turn around the cylindrical powdered samples. The values of B_1 differ by about a factor of 3 from the H_1 values generated in the transmitting coil without an Fe sample in place. Of course, we do not know what the real permeability or even the variation of it is in these samples; the factor 3 represents some kind of mean permeability under the conditions of operation. We will use B_1 in referring to the rf fields in the ferromagnetic materials so that this factor of 3 will not be incorporated into the enhancement factor which is of a different origin. That is, by enhancement factor we specifically mean the enhanced rf field which

TABLE II. Variation of resonance frequency of pure Fe with temperature.

Temp	Frequency (Mc/sec)
4.2°K	46.64
78°K	46.54
295°K	45.39

[12] M. Weger, thesis, University of California at Berkeley, 1961 (unpublished). Preliminary measurements of this type were made and discussed as part of Weger's thesis. His measurements do not agree with the results obtained here. However, they were a peripheral part of his work and thus not pursued with the degree of attentiveness given them here.

the nuclei see over that seen by the electrons. Since the nuclei in the domain-walls give rise to the observed signal, we are interested in the component of the rf field, which causes the wall to move. This is the projection of B_1 onto the direction of magnetization.[5] Thus, the effective field which causes the electron spins in the wall to move is $B_1 \cos\eta$. The Fe nuclei feel an enhanced field of the order $\epsilon B_1 \cos\eta$, where ϵ is the so-called enhancement factor. The value of $\epsilon[=\epsilon_0 f(x)]$ depends on the position x of the Fe nucleus in the wall. We shall see that we can obtain information on the variation of ϵ through the domain wall from the observed spectra. This variation is discussed below; at present, let us assume $\epsilon=\epsilon_0$. The direct rf field felt by the nuclei is negligible compared to the enhanced field since $\epsilon_0 \simeq aH_{\rm int}/H_A$, where $H_{\rm int}$, the internal magnetic field ($\simeq$330 kG), is much larger than H_A($\simeq$1.7 kG). The factor a is believed to be one in the domains but larger ($\sim$10–50) in the domain-walls because of the finite angle between adjacent atoms.[5,12] Since the width of the Fe^{57} NMR resonance ($\sim$50 kc) is small compared to the frequency spacings of the oscillations for most of the τ values used here, we shall neglect the Fe linewidth.

Thus, in the rotating frame, the field due to the applied rf which the nuclei experience is $\epsilon_0 B_1 \cos\eta$. Thus, θ and $b\tau$ are now given by

$$\tan\theta=\epsilon_0\gamma B_1(\cos\eta)/\Delta\omega, \tag{4}$$

$$b\tau=[(\Delta\omega)^2+(\epsilon_0\gamma B_1\cos\eta)^2]^{1/2}\tau. \tag{5}$$

During a pulse, the various nuclei precess through different angles depending upon the rf field which they feel. So we must now keep account of their phases. This is done by considering the x and y components in Eq. (1) separately. Also, during the FID the receiving coil detects the motion of the electrons which are coupled to the nuclei through the same factor, $\epsilon_0 \cos\eta$. Accordingly, we obtain for the FID amplitude

$$\mathfrak{A}(\omega, B_1, \tau)=\tfrac{1}{2}m_0\epsilon_0\left[\left(\int_0^\pi \sin\theta \sin b\tau \cos\eta \sin\eta d\eta\right)^2 + \left(\int_0^\pi \sin\theta \cos\theta(1-\cos b\tau) \cos\eta \sin\eta d\eta\right)^2\right]^{1/2}. \tag{6}$$

The factor $\frac{1}{2}$ comes from averaging over the azimuthal angle and normalizing. At resonance, $\theta=90°$, and Eq. (6) becomes

$$\mathfrak{A}(\omega_0, B_1, \tau)=\tfrac{1}{2}m_0\epsilon_0\int_0^\pi \sin(\alpha_0\cos\eta)\cos\eta\sin\eta d\eta, \tag{6'}$$

where $\alpha_0=\epsilon_0\gamma B_1\tau$ is the maximum turning angle. Equation (6′) has been evaluated with a computer and is shown plotted as a function of α_0 in Fig. 6. It is curve *a*. We see that averaging over the rf direction causes the oscillations to be damped. For protons, they would have varied as $\sin\alpha_0$.

b. Variation of ϵ with position in the domain wall. Lifshitz and Néel[13] have calculated the variation of spin direction across a static 90° domain-wall. Let the x axis be normal to the plane of the wall and let φ be the angle between the spin direction and the direction of domain magnetization z at a wall face. Considering the wall energy per unit area arising from the anisotropy and

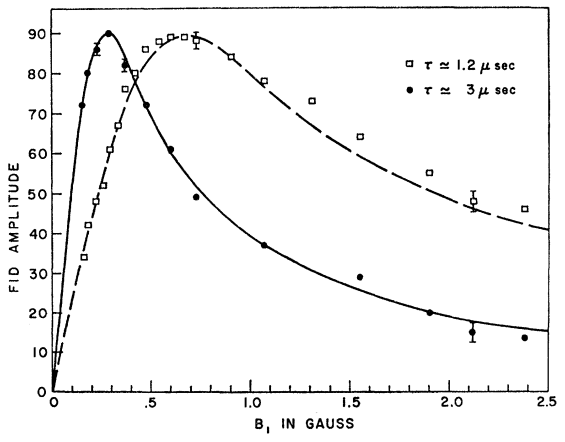

FIG. 5. Variation of the FID amplitude at resonance as a function of rf field B_1 for sample 1. The curves are calculated from Eq. (18″) (curve e of Fig. 6). The data for $\tau\simeq$1.2 μsec yield a maximum enhancement factor $\epsilon_0\simeq$7000, while that for $\tau\simeq$3 μsec give $\epsilon_0\simeq$6400.

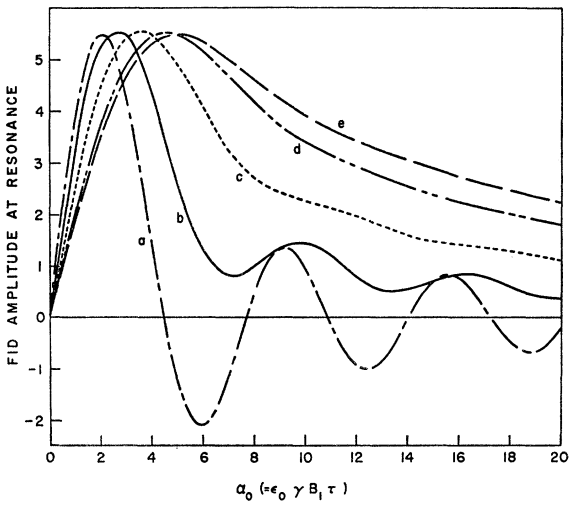

FIG. 6. Calculated curves of FID amplitude at resonance as a function of the maximum turning angle α_0. Each successively lettered curve shows the effects of an added phenomenon which contributes to the distribution of enhancement factors of the domain-wall nuclei. The accumulative effects are: (a) orientation of the rf field; (b) variation of the enhancement factor with position in the domain wall; (c) drumhead model with a constant area; (d) all domain-wall areas equally likely; (e) area variation, $A\,p(A)=$const.

[13] E. Lifshitz, J. Phys. USSR 8, 337 (1944); L. Néel, Cahiers Phys. 25, 1 (1944); See also C. Kittel and J. K. Galt, in *Solid State Physics*, edited by F. Seitz and D. Turnbull (Academic Press Inc., New York, 1956) Vol. 3, p. 437.

exchange energy densities, they obtained

$$dx=\delta d\varphi/\sin\varphi\cos\varphi, \tag{7}$$

where δ is a characteristic length of $\simeq$230 Å for Fe. The variation in the enhancement factor is given by $d\varphi/dx$, so that we have $\epsilon(\varphi)\sim(\sin\varphi\cos\varphi)/\delta$. From now on, let us measure x in units of δ. Taking the origin at the center of the wall; i.e., $x=0$ at $\varphi=45°$ we obtain a variation with x of

$$\epsilon(x)=\epsilon_0\,\mathrm{sech}x. \tag{8}$$

The variation of $\epsilon(x)$ derived above applies for static walls. Rado[14] has shown that for walls undergoing oscillatory motion of small amplitude, the angular variation with distance is essentially the same as for a static wall. Thus, Eq. (8) applies here.

In Fe, the effect of magnetostriction tends to decrease the distance between the centers of two 90° walls. In all the calculated examples given in this paper we have used an $\epsilon(x)$ given by Eq. (8). However, we have also investigated the effects on the FID amplitude of varying the distance between the centers of two 90° walls. We found, as might be expected, that small separations of from 0 to 0.5δ gave the best fits to the data.

Thus, including the enhancement factor variation, θ and $b\tau$ are given by

$$\tan\theta=(\epsilon_0\gamma B_1\,\mathrm{sech}x\cos\eta)/\Delta\omega$$

$$=(\alpha_0\,\mathrm{sech}x\cos\eta)/\Delta\omega\tau, \tag{9}$$

$$b\tau=[(\Delta\omega\tau)^2+(\alpha_0\,\mathrm{sech}x\cos\eta)^2]^{1/2}. \tag{10}$$

Thus, averaging over η and the variation in enhancement factors, we obtain for the FID amplitude

$$\mathfrak{A}(\omega, B_1, \tau)=\tfrac{1}{2}m_0\epsilon_0\left[\left(\int_0^\infty\int_0^\pi \sin\theta\sin b\tau \times\mathrm{sech}x\cos\eta\sin\eta d\eta dx\right)^2 +\left(\int_0^\infty\int_0^\pi \sin\theta\cos\theta(1-\cos b\tau)\,\mathrm{sech}x\cos\eta\sin\eta d\eta dx\right)^2\right]^{1/2}. \tag{11}$$

At resonance, Eq. (11) becomes

$$\mathfrak{A}(\omega_0, B_1, \tau)=\tfrac{1}{2}m_0\epsilon_0\int_0^\infty\int_0^\pi \sin(\alpha_0\,\mathrm{sech}x\cos\eta) \times\mathrm{sech}x\cos\eta\sin\eta d\eta dx. \tag{11'}$$

This is readily evaluated on a computer and shown plotted in Fig. 6 as curve b. We see that the variation in ϵ causes the oscillations of the FID amplitude to be more damped than before. Also, the amplitude no longer oscillates through zero. However, as seen in Fig. 5, the behavior is still far from that observed experimentally.

Similarly, there is still a large discrepancy between the behavior of the FID amplitude as a function of ω (fixed B_1 and τ) and that given by Eq. (11). Thus, representing the domain-walls as rigidly oscillating with proper account taken of their B_1 angular orientation and the enhancement-factor distribution due to the spacial arrangement of the spins in the domain wall does not agree well at all with the observed behavior of the FID amplitude.

At this point, A. W. Overhauser suggested that perhaps the domain-walls behaved more like vibrating membranes which were immobile around their peripheries, i.e., like drumheads.[15] An inherent consequence of this model is that the maximum enhancement factor should be smaller for the less pure Fe samples, as observed (see Table I). This results from the view that impurities augment domain nucleation and thus less pure samples have on the average more and smaller domains. At the intersections of these networks of domains, the walls are held immobile. As will now be discussed, this model indeed produces excellent agreement with the experimental results.

c. Drumhead model. Let us represent the domain-walls as circular membranes of radius r which are bound on their circumferences. The displacement of the nuclei in the direction perpendicular to the plane of the wall will then be proportional to $1-r^2$, where r varies from 0 to 1. The enhancement factor variation then becomes $\epsilon=\epsilon_0(\mathrm{sech}x)(1-r^2)$. Substituting this value for ϵ into the equations giving the FID amplitude at resonance, we get

$$\mathfrak{A}(\omega_0, B_1, \tau)=m_0\epsilon_0\int_0^1\int_0^\infty\int_0^\pi \sin(\alpha_0\,(\mathrm{sech}x)\,(1-r^2) \times\cos\eta)\,(\mathrm{sech}x)\,(1-r^2)\cos\eta\, r\sin\eta d\eta dx dr. \tag{12}$$

This assumes that all the domain-wall areas are equal. Equation (12) can be easily reduced to a double integration by using a joint distribution function. This is done in the Appendix. $\mathfrak{A}(\omega_0, B_1, \tau)$ can then be readily evaluated on a computer and is shown plotted in Fig. 6 as curve c. We see that the effect of this restricted motion is to further smooth the FID amplitude variation. But we still do not have good agreement with the experimental results.

However, there is another aspect of the domain-wall drumheads that should be considered, namely, their distribution in areas. The dependence of the maximum displacement h_m upon the wall area is obtained as

[14] G. T. Rado, Phys. Rev. **83**, 824 (1951).

[15] It was brought to the attention of the author after this work was completed that A. Globus has proposed a model containing somewhat similar features to explain the dependence of the initial susceptibility on grain size in ferrites. See A. Globus and P. Duplex, IEEE Trans. Mag. **2**, 441 (1966).

follows. The surface energy expended in bowing out the wall is $\sigma_w \Delta A$, where σ_w is the surface energy per unit area and $\Delta A (=\pi h_m^2)$ is the increase in area of the wall. The interaction energy with the rf field is $-B_1 \Delta M$, where ΔM is the change in magnetization caused by the moving wall. It is given by $\Delta M = 2M_s \Delta V$, where M_s is the saturation magnetization. The volume change is given by $\Delta V = \frac{1}{2}\pi h_m a^2$, where a is the radius of the circular-domain-wall segment. Thus, the energy change due to the bowing out of the domain wall is given by

$$\Delta E = \sigma_w \pi h_m^2 - B_1 M_s \pi h_m a^2. \tag{13}$$

Minimizing this with respect to h_m gives

$$h_m = (B_1 M_s / 2\sigma_w) a^2. \tag{14}$$

Consequently, the maximum displacement of a moving wall is proportional to its area and the probability distribution of h_m is the same as the probability distribution of domain-wall areas. What concerns us, however, is the probability $p(h_m)$ of a nucleus being in a domain-wall segment having a maximum displacement h_m. Since the number of nuclei in a domain-wall of area A is proportional to A, $p(h_m)$ varies as $Ap(A)$. Thus, we obtain an enhancement factor variation for the domain-wall nuclei of

$$\epsilon = \epsilon_0 (\mathrm{sech} x)(1-r^2) h_m, \tag{15}$$

where h_m is always normalized to 1, i.e., we measure h_m in units of the maximum value of h_m. We thus implicitly assume a maximum area for the domain-wall segments. Its value has no effect on the form of the equations derived here, but is directly incorporated in the value of ϵ_0. This is as expected since larger area segments oscillate through greater excursions and thus have larger average enhancement factors.

The expression for θ and $b\tau$ now become

$$\tan\theta = [\alpha_0 (\mathrm{sech} x)(1-r^2) h_m \cos\eta]/\Delta\omega\tau, \tag{16}$$

$$b\tau = [(\Delta\omega\tau)^2 + [\alpha_0 \,\mathrm{sech} x (1-r^2) h_m \cos\eta]^{1/2}. \tag{17}$$

The FID amplitude then becomes

$$\mathfrak{A}(\omega, B_1, \tau) = m_0\epsilon_0 \left\{ \left[\int_0^1 \int_0^1 \int_0^\infty \int_0^\pi \sin\theta \sin b\tau \,\mathrm{sech} x \,(1-r^2) h_m \cos\eta p(h_m) r \sin\eta d\eta dx dr dh_m \right]^2 \right.$$
$$\left. + \left[\int_0^1 \int_0^1 \int_0^\infty \int_0^\pi \cos\theta (1-\cos b\tau) \,\mathrm{sech} x (1-r^2) h_m \cos\eta p(h_m) r \sin\eta d\eta dx dr dh_m \right]^2 \right\}^{1/2} \tag{18}$$

These multiple integrations can again be reduced to double integrations by using joint distribution functions. This is shown in the Appendix. Defining $z = (1-r^2) h_m \cos\eta$ we obtain

$$\mathfrak{A}(\omega, B_1, \tau) = \tfrac{1}{2} m_0 \epsilon_0 \left\{ \left[\int_0^\infty \int_0^1 (\sin\theta \sin b\tau \,\mathrm{sech} x \, z p(z) dz dx \right]^2 + \left[\int_0^\infty \int_0^1 \cos\theta (1-\cos b\tau) \,\mathrm{sech} x \, z p(z) dz dx \right]^2 \right\}^{1/2}, \tag{18'}$$

where $p(z)$ is the probability density function of z as given in the Appendix. At resonance, the FID amplitude becomes

$$\mathfrak{A}(\omega_0, B_1, \tau) = \tfrac{1}{2} m_0 \epsilon_0 \times \int_0^\infty \int_0^1 \sin(\alpha_0 z \,\mathrm{sech} x) z \,\mathrm{sech} z p(z) dz dx. \tag{18''}$$

There are two simple and reasonable area variations which are easy to evaluate. They are: (1) All domain-wall areas are equally likely, i.e., $p(A) = \text{const}$ (up to the maximum area). Here $p(h_m)$ is proportional to h_m. (2) $p(A)A = \text{const}$, i.e., the probability of having a given area A varies as $1/A$. Here $p(h_m)$ is a constant.

In the Appendix we evaluate $p(z)$ for each of these area distribution assumptions. Equation (18″) can then be evaluated with a computer, and the results are shown in Fig. 6. Curve d is for $p(A) = \text{const}$ and curve e is for $Ap(A) = \text{const}$. Both of these area variations give agreement with the measured variation of the FID amplitude at resonance, the second giving a somewhat better fit. Thus, we find that while the results are not too sensitive to the type of domain-wall variation, some such variation must be included to obtain agreement with the experimental data.

4. *Comparison of Measured and Calculated Results*

Figure 5 shows the comparison of the calculated curves with the measured FID amplitude at resonance. The curves shown are obtained from curve e of Fig. 6. The abscissa of curve e is scaled to give the best fit to each set of data. Each curve thus yields a value of ϵ_0. The $\tau \simeq 1.2$ μsec curve corresponds to an $\epsilon_0 \simeq 7000$, while the $\tau \simeq 3$ μsec data give an $\epsilon_0 \simeq 6400$.

We should expect at least two separate effects to influence the average domain-wall area. One has already been mentioned, namely, that of impurities augmenting domain nucleation and thus producing on the average more and smaller domain-wall-area segments. This manifests itself as a decrease in the maximum enhancement factor for less pure samples. (See Table I). The second is the well-known effect of the pinning of the domain walls due to impurities, imperfections, etc. This effect is expected to exhibit a temperature dependence.

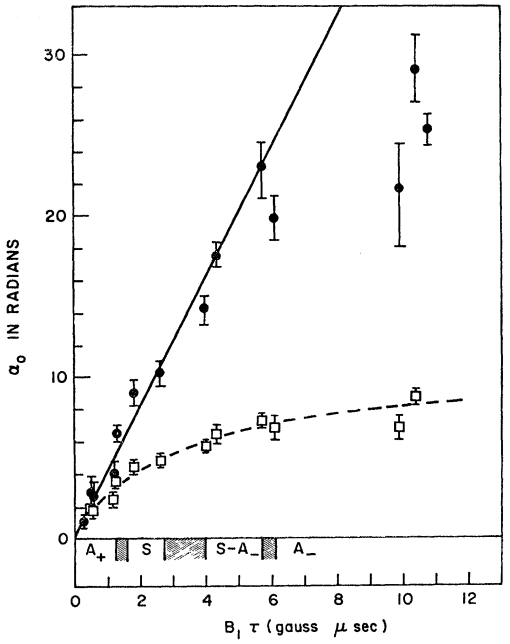

FIG. 7. Variation of the spectral shape parameter α_0 with $B_1\tau$ for sample 1. The squares are from spectra calculated with model b (no drumheads). The circles are from spectra calculated with model e [drumheads with an area distribution given by $Ap(A)=$const]. For the correct model, the data should fall on a straight line.

At higher temperatures, we should have less pinning and therefore larger domain-wall segments, thus resulting in an increase in the maximum enhancement factor. This behavior of ϵ_0 has been observed in sample 1. The values of ϵ_0 obtained from type-II measurements at various temperatures are listed in Table I. We see that the maximum enhancement factor is about three times greater at room temperature than at He temperature.

Let us now compare the calculated spectra with the measured spectra. The spectra are taken with B_1 and τ fixed, so that the only parameter determining the spectral shape is $\alpha_0(=\epsilon_0\gamma B_1\tau)$. On the right-hand side of Fig. 4 we show some calculated spectra from the drumhead model given by Eq. (18′) with $Ap(A)=$ const. The FID amplitude $\mathcal{A}(\omega)$ is shown plotted versus $\Delta\omega\tau$ in radians. Thus, for a given model, we can compute a family of spectral curves and by comparing these with the measured spectra, assign to each measured spectrum a value of α_0. The known value of $B_1\tau$ characterizes each measured spectrum. We show plotted in Fig. 7 the values of α_0 obtained in this way versus the $B_1\tau$ of the measured spectra for sample 1. The squares correspond to the α_0 values obtained from spectra calculated for the model taking into account only the B_1 orientation and variation of ϵ with position in the wall (model b of Fig. 6). The solid circles correspond to the α_0 values obtained from the drumhead model with the area variation $Ap(A)=$const (model e of Fig. 6). For a correct model, we expect the data to fall on a straight line with slope equal to $\gamma\epsilon_0$. We see that the data from the drumhead model meet this criterion fairly well except at high $B_1\tau$ values, where we might expect deviations. Indeed, in Fig. 4 we can see that the agreement between the spectra calculated from model e and the measured spectra is excellent. However, asymmetries are present; these are discussed below. Model b without drumhead motion of the walls obviously gives a very poor fit to the measured spectra. The value of ϵ_0 obtained from the slope of the drumhead model data is 5 000–6 000.

5. *Asymmetries*

The measured spectra in Fig. 4 show some distinctive asymmetries at high and low values of $B_1\tau$. The general regions and types of asymmetry are shown along the abscissa of Fig. 7. For values of $B_1\tau$ less than 1.25 G-μsec, the spectra had asymmetries as shown in curve d of Fig. 4. That is, the high-frequency side was of greater amplitude than the low-frequency side. This is referred to as an $A+$ asymmetry in Fig. 7. In this region the asymmetry was dependent on the product $B_1\tau$ but was independent of the values of B_1 and τ; i.e., a spectrum with $B_1=0.2$ G and $\tau=6.5$ μsec had about the same degree of asymmetry as one with $B_1=0.9$ G and $\tau=1.35$ μsec. For $B_1\tau$ between 1.6 and 2.6, the observed spectra were very symmetrical. For $B_1\tau$ from 4 to 6.7, the spectra were quite symmetrical with a slight $A-$ asymmetry. An $A-$ asymmetry is one where the low-frequency side has the larger amplitude. Above $B_1\tau=$ 6.1 G-μsec the spectra were $A-$ asymmetrical as typified by curve a in Fig. 4. In this high-$B_1\tau$ region there also seemed to be a B_1 dependence. That is, for the same $B_1\tau$ value, the higher B_1 spectra were more asymmetrical. The asymmetries are not understood although there are several reasons why they might

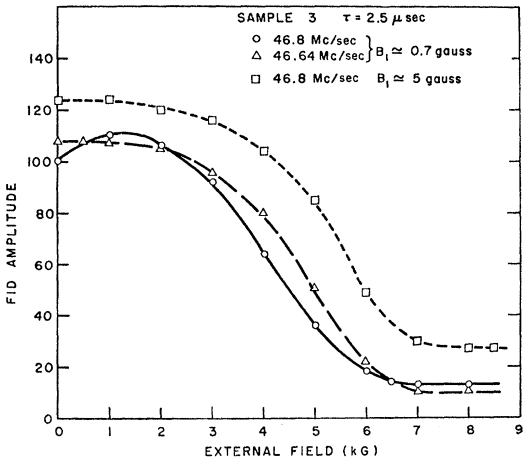

FIG. 8. Relative FID amplitudes for sample 3 as a function of external magnetic field. The exciting rf frequencies were equal to the resonance frequency, 46.64 Mc/sec, and the frequency of the first maximum, 46.8 Mc/sec.

occur. (1) At large B_1 the maximum displacement h_m of the wall may be sizeable compared to the wall thickness. If so, the wall motion would no longer have a linear dependence on B_1. We indeed observed that there was some B_1 dependence in the $A-$ region. From Eq. (14) we can estimate the values of h_m. For Fe, $\sigma_w \simeq 1.8$ erg/cm^2 and $M_s \simeq 1.7$ kG. We expect drumhead radii of from 0.1 μ or less to perhaps as large as a few microns in very pure material. For $B_1=1$ G and a 0.1 μ radius, we obtain $h_m \sim 5$ Å. This would be in the linear displacement region since the wall thickness in Fe is ~ 1000 Å$_0$. However, a 1 μ radius would give $h_m \sim 500$ Å. Here, the domain-wall motion should have a very nonlinear dependence on B_1 which might well produce asymmetries. (2) We have neglected completely the counter-rotating component of B_1; this might produce some asymmetry especially in the low-$B_1\tau$ region. (3) The domain-wall drumheads will have a series of resonances. If we were near such a resonance, we would expect to obtain asymmetrical spectra. We can estimate the domain-wall-resonance-frequencies as follows: Neglecting the effects of damping on the domain-wall mass, the resonance frequency of a drumhead of radius a is given by

$$\omega_n = (x_n/a)(\sigma_w/m_w), \tag{19}$$

where x_n is the nth zero of the Bessel function $J_0(x_n)$ and m_w is given by $m_w = (1/4\pi\gamma^2)(K/A)^{1/2} \simeq 1.1 \times 10^{-10}$ gm/cm^2 for Fe. Thus, the lowest domain-wall frequency is $\omega \simeq (3.1 \times 10^5)/a$. For $a=0.1$ μ this gives

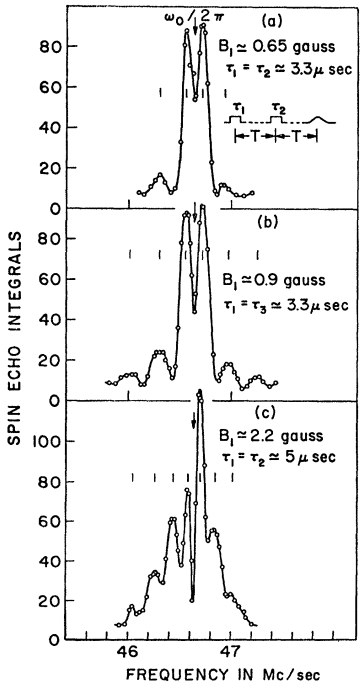

FIG. 9. Some typical spectra of the spin-echo integral as a function of the transmitting frequency.

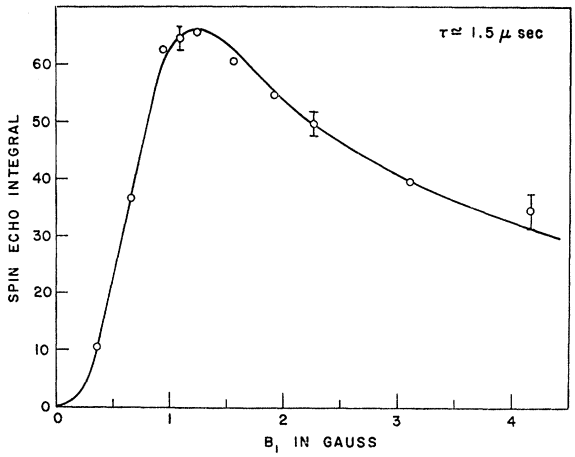

FIG. 10 Variation of the spin-echo amplitude at resonance as a function of the rf field B_1 for sample 1. The curve is calculated from Eq. (21′) as discussed in the text.

$\sim 5 \times 10^9$ cps. This is much larger than the frequencies at which we operate $\sim 5 \times 10^7$ cps and thus we would expect that none of the asymmetry effects arises from the domain-wall resonances. However, if the domain-wall radii are larger and the damping causes an increase in m_w, the wall-resonances frequencies would be lower.[16]

6. *Measurements Made In An External dc Field*

A series of measurements was also made with an external dc field applied perpendicular to the axis of the rf coils. As the field was increased, the shape of the measured FID spectra remained about the same but the intensity decreased. This behavior was the same for all three Fe samples. Figure 8 shows the variation of the intensity of the FID with external field at resonance, 46.64 Mc/sec, and at the first maxima, 46.8 Mc, for sample 3 which consisted of spheres with diameters of 3–5 μ. We see in Fig. 8 that the signal disappears at about 7 kG, which corresponds closely to the field value at which we would expect all the walls to be swept away. It has been suggested by Weger[12] and Bennett[17] that there is a decrease in enhancement factor with applied external dc fields. To investigate this more carefully, we measured the enhancement factor for sample 2 as a function of external dc field by type-II measurements. With $\tau \simeq 1.5$ μsec we measured the FID amplitude as a function of B_1 in external dc fields of 0, 1.35, 2, 4, and 4.8 kG. We observed no change in the

[16] Note that the drumhead model gives a domain-wall resonance frequency which is dependent on the domain-wall radii. Since we have a distribution in these radii, we will also naturally have a spread in wall frequencies. We would thus expect a broad resonance in the "magnetic spectra" (frequency dependence of the complex initial permeability) of ferromagnetic material. Such behavior has often been observed in ferrites but not understood. See, for example, G. T. Rado, Rev. Mod. Phys. **25**, 81 (1953) and G. T. Rado, R. W. Wright, and W. H. Emerson, Phys. Rev. **80**, 273 (1950).

[17] L. H. Bennett, J. Appl. Phys. **37**, 1242 (1966).

value of B_1 at the maximum FID amplitude over the whole range. This indicates that the enhancement factor is the same in external dc fields from 0 to 4.8 kG. The measured enhancement factor was ~2800.

IV. SPIN ECHOES IN Fe

A. Measured Spectra

Although the FID is easier to measure and interpret than the echo in pure Fe, in alloys, where the width of the resonance line is much greater than that in pure Fe, the FID time is so short that most of it occurs during the 3–5 μsec dead time of the receiver. In these cases, it is necessary to look at the echos. For the echos we usually kept both rf pulses the same width. The time between pulses was kept large compared to the FID time (15–20 μsec) and was usually around 250 μsec. The results were not sensitive to reasonable variations of this time. It was observed that the shape of the echo changed as the exciting rf frequency varied, especially near resonance. Here, the shape no longer resembled two back-to-back FID's, but broke up into several maxima and minima. For this reason, we usually made measurements on the integral of the echo. A gated integrator with an RC of about 40 μsec was used to integrate any signal occurring within a time of about 80 μsec centered around the echo. Echo-height measurements were also made and the results were essentially the same when care was taken that the maximum height was measured. Measurements of the echo were made at liquid He and N_2 temperatures. Figure 9 shows some typical echo spectra for sample 1 at 4.2°K. Since the detected signal was always at ω_0 and the receiver gain was essentially independent of the transmitting frequency, no corrections of the spectra were necessary. Note that the spectra have a much smaller frequency extent than the FID spectra; the echo in curve c has about the same $B_1\tau$ as curve a of the FID spectra.

Type-II measurements of the spin-echo integral at resonance as a function of rf field were also taken. Figure 10 shows some typical results for $\tau=1.5$ μsec. The curve shown was calculated as discussed below.

B. Echo Calculations

We shall calculate the echo amplitude under the same assumptions as were used to calculate the FID amplitude. The first pulse rotates the nuclear magnetization through an angle $b\tau_1$ around the vector **b**. After the pulse is turned off, the nuclei freely precess about $\mathbf{H}_{\text{int}}$ for a time T. Because of their spread in resonant frequencies, they become uniformly spread out in the x-y plane. The second pulse then again rotates the z components through an angle $b\tau_2$ around **b** and we observe the echo at time $2T$. Jaynes and Bloom[18] have developed an elegant matrix method to obtain the echo amplitude after any series of pulses. We can use their formulas directly. We apply Eq. (3) of Bloom's paper for the case $\tau_1=\tau_2$. (Therefore, $\alpha_1=\alpha_3$, $\beta_1=\beta_3$ in Bloom's notation.) The echo amplitude $\mathcal{E}(\omega)$ is given by $G_2G_2^*$, where G_2 is given by Eq. (14) of Bloom's paper. Therefore, for protons, we would obtain

$$\mathcal{E}(\omega)=m_0 \sin\alpha \sin^2\theta \sin^2\tfrac{1}{2}b\tau. \tag{20}$$

Substituting in the value of $\sin\alpha$ given by Eq. (1) we obtain

$$\mathcal{E}(\omega)=m_0 \sin^3\theta \sin^2\tfrac{1}{2}b\tau[\sin^2(b\tau)+\cos^2\theta(1-\cos b\tau)^2]^{1/2}. \tag{20'}$$

To get agreement with the experimental results, it is again necessary to take into account all the effects which we found to be present for the FID-amplitude calculations. That is, we consider: (1) the B_1 orientation and average over angle η, (2) the spread in ϵ through the domain wall, (3) the drumhead-like motion of the domain walls with an area distribution of $Ap(A)=$ const. The values of θ and $b\tau$ are given by Eqs. (16) and (17). Again, using the joint-distribution function as given in the Appendix, we obtain for the echo amplitude

$$\mathcal{E}(\omega, B_1, \tau)=\tfrac{1}{2}m_0\epsilon_0\left[\left(\int_0^\infty\int_0^1 \sin^3\theta \sin^2\tfrac{1}{2}(b\tau)(\sin b\tau)z \operatorname{sech}x\, p(z)dzdx\right)^2 + \left(\int_0^\infty\int_0^1 \sin^3\theta \sin^2\tfrac{1}{2}(b\tau)\cos\theta(1-\cos b\tau)z \operatorname{sech}x\, p(z)dzdx\right)^2\right]^{1/2}. \tag{21}$$

At resonance this becomes

$$\mathcal{E}(\omega_0, B_1, \tau)=\tfrac{1}{2}m_0\epsilon_0\int_0^\infty\int_0^1 \sin^2\tfrac{1}{2}(\alpha_0 z \operatorname{sech}x)\sin(\alpha_0 z \operatorname{sech}x)z \operatorname{sech}x\, p(z)dzdx, \tag{21'}$$

[18] E. T. Jaynes, Phys. Rev. **98**, 1099 (1955); A. L. Bloom, *ibid.* **98**, 1105 (1955). Many of the particular formulas given in the second paper apply at resonance only, so they have to be altered properly to use off resonance.

where $p(z)=\frac{1}{2}\ln^2(1/z)$ for $Ap(A)=\text{const}$. Both of these echo amplitudes can be readily evaluated on a computer and compared with the experimental results.

C. Comparison of Experimental and Calculated Echo Amplitudes

The curve shown in Fig. 10 is obtained from Eq. (21′). We see that it agrees excellently with the measured echo integral at resonance.

Typical calculated echo spectra are shown plotted in Fig. 11. In order to compare them with the FID spectra, we have chosen values of α_0 close to those shown plotted on the right-hand side of Fig. 4. We see that the echo spectra are much less extensive. The relative maximum values of the FID and echo spectra are in a ratio of about 2.3 to 1. Thus, the FID amplitude is larger, more extensive, and simpler to calculate. By comparing the measured echo spectra with the calculated spectra we can again obtain values of α_0 for the measured spectra. For the same $B_1\tau$ the α_0 values obtained from the echo spectra agreed with those obtained from the FID spectra. The echo values, however, are not as reliable as those obtained from FID spectra.

We can see from Fig. 9 that the echo spectra also have asymmetries. Here, however, the type of asymmetry was always the same and the spectra were more asymmetrical at higher $B_1\tau$. The first peak on the high-frequency side was always larger than the first peak on the low-frequency side, while all the other peaks on the low-frequency side were larger than their corresponding peaks on the high-frequency side. The asymmetry tended to decrease at low $B_1\tau$ but never was observed to completely disappear. This type of asymmetry does not seem to correspond to either type observed in the FID spectra. Since the origin of the echo is more complicated than that of the FID, we would expect more pronounced and complex asymmetries in echo spectra than in the FID spectra.

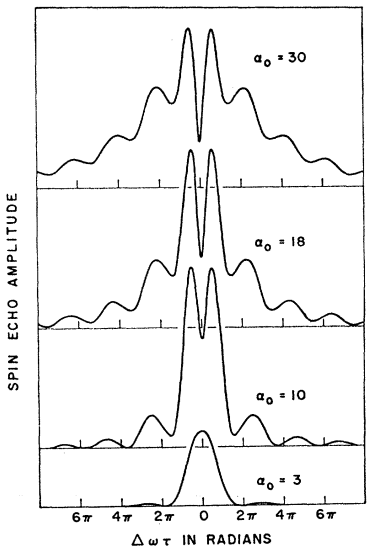

FIG. 11. Spectra of the spin-echo amplitude as a function of $\Delta\omega\tau$ calculated from Eq. (21). The domain-wall motion is represented by circular drumheads with an area variation as discussed in the text.

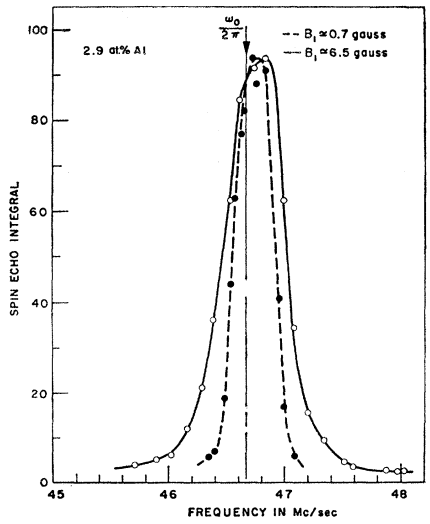

FIG. 12. Spin-echo integral of a 2.9 at. % Al alloy as a function of exciting frequency. The conditions of operations were: 4.2°K, $\tau_1=\tau_2\simeq 15$ μsec, $T=250$ μsec, integration time $=50$ μsec, RC of integrator $=1$ μsec. There is also a satellite centered around 43.5 Mc/sec which is not shown.

Thus, we find that we can obtain the same information from echo measurements as from FID measurements. However, the echo results are less accurate and thus less desirable to use.

V. SPIN ECHOES IN ALLOYS

In Mössbauer experiments, it has been observed that Fe rich binary ferromagnetic alloys[4] fell into two classes. In the first, the Mössbauer spectra showed structure in the individual lines and the magnetic effects due to the solute atoms looked localized. In the second, there was no structure present, as if the magnetic effects due to the solute atoms were nonlocalized. Here, we studied the spin echoes of a typical alloy from each class: the first, FeAl; the second, FeCo. The linewidths of both alloys were very broad compared to the pure Fe samples as evidenced by the free-induction-decay time. It was about 1 μsec or less for alloys of 1 at.% or more Al and 2–3 μsec for a 1 at.% Co alloy.

A. "Localized" Solute Atoms

When the magnetic effects of the solute atoms are localized, we expect the internal magnetic field of the neighboring nuclei to vary depending on the occupational configuration of each Fe atom. The free-induction-decay time indicates the spread in fields at the Fe

TABLE III. Enhancement factor for various alloys.

At.%	ϵ	Frequency (Mc/sec)
3.8 Al	~400	46.64
3.8 Al	~400	43.5
4.8 Si	~480	46.64
1.0 Co	~600	46.64

atoms is at least about 1 Mc/sec or 7 kG. Figure 12 shows the echo amplitude as the exciting frequency is varied for a 2.9 at.% Al alloy. No gain corrections as a function of frequency have been made here. The gain corrections would be the same for both curves and modify the curves only slightly. Since we have a large spread in internal fields, we expect the oscillations and hole to be washed out, as observed. There is also a small peak at 43.5 Mc/sec which we do not show; it corresponds to those Fe atoms with one nearest-neighbor Al atom.[3,4] It is evident from Fig. 12 that we have a large asymmetry about ω_0. We also note that the spectra get broader at the higher power just as observed in Fig. 9 for pure Fe and as they should from Eq. (21). Although we do not see any hole at 46.64 Mc/sec, we can still use the second method to measure the maximum enhancement factor, i.e., measure the echo-amplitude variation with rf field at the resonance frequency for a given τ. Such measurements yield curves similar to those shown in Fig. 10. From the maximum we obtain the α_0 which corresponds to a known $B_1\tau$, and thus find ϵ_0. Values of ϵ_0 obtained in this way are listed in Table III for a 3.8 at.% Al and a 4.8 at.% Si alloy. We also measured the enhancement factor of the Fe atoms with one nearest-neighbor solute atom by a type-II measurement at 43.5 Mc/sec. We found that such Fe atoms have essentially the same value of ϵ_0 as Fe atoms with no nearest-neighbor Al atoms (see Table III). This is of interest because the fraction of Fe atoms in this alloy with nearest-neighbor Al atoms is only about 0.4%. The equality of the ϵ_0's thus indicates that the magnetic electron system in the domain-wall is indeed very tightly coupled.

B. FeCo

Mössbauer experiments have indicated that all of the Fe atoms have very nearly the same internal field in FeCo. Thus, we expected the same type of spectrum here as we observed for pure Fe. Figure 13 shows the variation of the integral of the spin echo with frequency of an alloy with 1 at.% Co in Fe. No corrections for gain change with frequency were necessary since the echo frequency is assumed to be ω_0. We did indeed observe all the features observed in the echo of pure Fe:, i.e., the hole digging at ω_0, the asymmetry around ω_0, and the oscillations having a spacing of $1/\tau$. The structure reported earlier[3] for this alloy probably is due to this behavior rather than indicating discrete variations of internal fields at the Fe nuclei in this alloy. We also measured the maximum enhancement factor by a type-II measurement at resonance. We obtained curves similar to Fig. 10 and from these found $\epsilon_0 \sim 600$.

From the enhancement-factor values measured in this work, it appears that substitutional solute atoms produce lower maximum-enhancement factors than interstitial impurities. This may be because the interstitial impurities tend to cluster; in fact, the structure of the GAF spherical Fe samples, 2 and 3, is supposedly of an "onion-skin" character with alternating layers of Fe and impurity atoms.

Thus, for a well-separated satellite, like one from Fe atoms with a nearest-neighbor Al atom, one can obtain a value for the internal-field shift. However, it is questionable whether the intensity of the satellite can be measured with much accuracy. We see that in measuring the line shape as a function of frequency, the rf level should not be changed at the various frequencies since this changes the resolution of the apparatus. It had been hoped that for Fe, spin-echo techniques would have an inherent resolution at least a factor of 10 better than the Mössbauer resolution, and therefore they would provide an accurate method for obtaining the variation of the internal field due to higher than nearest-neighbors solute atoms. However, the complex structure, and especially the asymmetries in the spectra make the unfolding of the spectra into components due to various neighbor shells unfeasible at present.

VI. CONCLUSIONS

In these measurements, the NMR signal arises from the nuclei in the domain walls. For pure Fe samples,

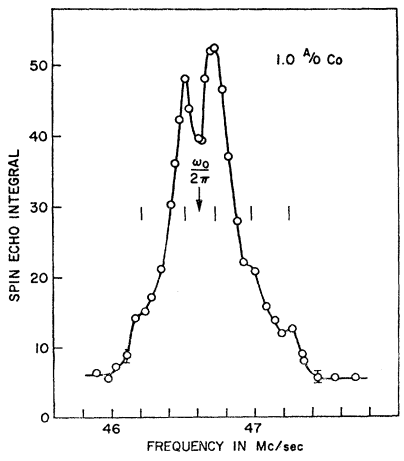

FIG. 13. Spin-echo integral of 1.0 at. % Co alloy as a function of exciting frequency. The conditions of operation were: 4.2°K, $B_1 \simeq 5.5$ G $\tau_1 = \tau_2 \simeq 3$ μsec, $T = 80$ μsec, integration time = 50 μsec, RC of integrator = 30 μsec. The structure in this alloy is due to the turning-angle effects as discussed for pure Fe.

there is a sufficient range of values of $B_1\tau$, where the FID spectra are quite symmetrical and well behaved enough so that we can ascertain a consistent model of domain-wall motion. To obtain agreement with the experimental results requires a model that encompasses the following features:

(1) An averaging over the spatial orientation of the local magnetization directions with respect to the applied rf field.

(2) The variation of the enhancement factor with position perpendicular to the plane of the domain-wall due to the spin arrangement in the wall.

(3) The domain-wall is composed of segments which are immobile around their perimeters and whose motion resembles that of a vibrating drumhead. These segments have a distribution in areas. On the average, the areas are smaller the less pure the Fe sample and larger the higher the temperature. Spin-echo measurements confirm the above features, but this technique is more complex and gives less accurate results than the FID measurements.

The maximum enhancement factor does not vary appreciably for externally applied dc magnetic field up to around 5 kG.

The same features are seen in the echoes of the alloys as in pure Fe. This makes an unfolding of the spectral shapes of the alloys in terms of the effects due to the neighboring solute atoms (except where the satellites are far removed from the main line) a very dubious procedure.

ACKNOWLEDGMENTS

It is a pleasure to thank A. W. Overhauser for many cardinal suggestions and enlightening discussions, and also T. Kushida for the gracious loan of many of the electronic components used in these experiments as well as many instructive conversations.

APPENDIX: JOINT DISTRIBUTION FUNCTIONS

We want to find the joint distribution function needed to replace the integrations over r and η by a single integration. Let

$$w=(1-r^2)\cos\eta \tag{A1}$$

and

$$u=1-r^2 \qquad 0\leq r\leq 1. \tag{A2}$$

Then from

$$p(u)\,du=p(r)\,dr=2r\,dr,$$

we find

$$p(u)=1 \quad \text{for} \quad 0\leq u\leq 1. \tag{A3}$$

Similarly, if

$$v=\cos\eta, \tag{A4}$$

then

$$p(v)=1 \quad \text{for} \quad 0\leq v\leq 1. \tag{A5}$$

The joint distribution function is given by

$$p(w)\,dw=\int_w^1 p\left(\frac{w}{v}\right)p(v)\,dv\,\frac{dw}{v}, \tag{A6}$$

where u is evaluated at w/v. Substituting in Eqs. (A3) and (A5), we find the probability density function of w,

$$p(w)=\ln(1/w) \quad \text{for} \quad 0\leq w\leq 1. \tag{A7}$$

Eq. (13) thus becomes

$$\mathcal{G}(\omega_0, B_1, \tau)=\tfrac{1}{2}m_0\epsilon_0\int_0^\infty\int_0^1 \sin(\alpha_0 w\,\mathrm{sech}x)\,w \times\mathrm{sech}x\ln\left(\frac{1}{w}\right)dw\,dx. \tag{A8}$$

Next, we want the joint distribution function of

$$z=h_m w. \tag{A9}$$

This is again given by

$$p(z)\,dz=\int_z^1 p\left(\frac{z}{w}\right)p(w)\,dw\,\frac{dz}{w}, \tag{A10}$$

where h_m is evaluated at z/w. For case 1, of equal probabilities for all domain-wall areas, $p(h_m)=2h_m$ and

$$p_1(z)=2[\ln(1/z)+z-1] \quad \text{for} \quad 0\leq z\leq 1. \tag{A11}$$

For case 2, where $Ap(A)=\text{const}$, $p(h_m)=1$ for $0\leq h_m\leq 1$ and

$$p_2(z)=\tfrac{1}{2}\ln^2(1/z) \quad \text{for} \quad 0\leq z\leq 1. \tag{A12}$$